Repurposing clemastine to target glioblastoma cell stemness

Michael A. Sun[1,2,3,#], Rui Yang[1,2,#], Heng Liu[1,2,3], Wenzhe Wang[1,2], Xiao Song[4], Bo Hu[4], Nathan Reynolds[1,2], Kristen Roso[1,2], Lee H. Chen[1,2], Paula K. Greer[1,2], Stephen T. Keir[1,5], Roger E. McLendon[1,2], Shi-Yuan Cheng[4], Darell D. Bigner[1,5], David M. Ashley[1,5], Christopher J. Pirozzi[1,2,*], Yiping He[1,2,*]

[1]The Preston Robert Tisch Brain Tumor Center, Duke University Medical Center, Durham, NC 27710, USA

[2]Department of Pathology, Duke University Medical Center, Durham, NC 27710, USA

[3]Pathology Graduate Program, Duke University Medical Center, Durham, NC 27710, USA

[4]The Ken & Ruth Davee Department of Neurology, Lou and Jean Malnati Brain Tumor Institute, The Robert H. Lurie Comprehensive Cancer Center, Simpson Querrey Institute for Epigenetics, Northwestern University Feinberg School of Medicine, Chicago, IL 60611, USA

[5]Department of Neurosurgery, Duke University Medical Center, Durham, NC 27710, USA

Contribute equally

* Corresponding Author:

Yiping He, PhD
203 Research Drive, Medical Science Research Building 1, Room 199A
Duke University Medical Center, Durham, NC 27710
Phone: (919) 684-4760
Email: yiping.he@duke.edu

Christopher J. Pirozzi, PhD
203 Research Drive, Medical Science Research Building 1, Room 199B
Duke University Medical Center, Durham, NC 27710
Phone: (919) 684-5971
Email: christopher.pirozzi@duke.edu

Keywords: clemastine, glioblastoma, stemness, Emopamil Binding Protein (EBP)

Abstract

Brain tumor-initiating cells (BTICs) and tumor cell plasticity promote glioblastoma (GBM) progression. Here, we demonstrate that clemastine, an over-the-counter drug for treating hay fever and allergy symptoms, effectively attenuated the stemness and suppressed the propagation of primary BTIC cultures bearing *PDGFRA* amplification. These effects on BTICs were accompanied by altered gene expression profiling indicative of their more differentiated states, resonating with the activity of clemastine in promoting the differentiation of normal oligodendrocyte progenitor cells (OPCs) into mature oligodendrocytes. Functional assays for pharmacological targets of clemastine revealed that Emopamil binding protein (EBP), an enzyme in the cholesterol biosynthesis pathway, is essential for BTIC propagation and a target that mediates the suppressive effects of clemastine. Finally, we showed that a neural stem cell-derived mouse glioma model displaying predominantly proneural features was similarly susceptible to clemastine treatment. Collectively, these results identify pathways essential for maintaining the stemness and progenitor features of GBMs, uncover BTIC dependency on EBP, and suggest that non-oncology, low-toxicity drugs with OPC differentiation-promoting activity can be repurposed to target GBM stemness and aid in their treatment.

Introduction

Glioblastoma (GBM) tumors demonstrate striking aggressiveness and therapeutic resistance, which are driven by brain tumor-initiating cells (BTICs), a subpopulation of GBM cells that exhibit phenotypic plasticity and stem/progenitor-like features[1-6]. The pathological ramifications of GBM plasticity and stemness are highlighted by the heterogeneous nature of GBM with the presence of various subtypes, including proneural (PN), classical (CL), and mesenchymal (MES) subtypes[7-12]. Among the GBM subtypes, the PN tumors are characterized by stem/progenitor-like signatures, failure to respond to more aggressive chemo- and radio-therapy[9,13], and the ability to undergo the process of proneural-mesenchymal transition (PMT)[14,15]. Facilitated and driven by GBM plasticity and stemness, these tumors can transition from one subtype to another in the course of tumor progression and recurrence, and give rise to the most aggressive tumors with the worst prognosis, the MES subtype GBMs[9,13]. In addition, a previous study has provided evidence to suggest that the PN-like precursor cells can serve broadly as progenitors for GBMs and give rise to various subtypes of tumor cells[16]. Collectively, these findings support targeting GBM cell stemness as a strategy for mitigating GBM progression.

Numerous studies have provided critical insights into the mechanism of stemness maintenance in GBM[17-21], and offered promising strategies, including epigenetic and metabolic approaches, for targeting this property of GBM cells[22-27]. One alternative strategy for targeting stemness and plasticity of cancer cells is to promote their differentiation, an approach that has seen great promise in blood cancers[28]. Although employing this strategy for solid tumors has proven more complicated, recent studies have supported the feasibility of attenuating tumor cells' stemness/plasticity features and mitigating tumor progression in solid tumors via inducing their differentiation[29-31]. In gliomas, IDH1 mutant-induced differentiation blockage has been exploited for therapeutic purposes[32,33], and metabolism-based strategies for directing GBM differentiation have been proposed[34,35]. In addition to the benefit of attenuating stemness, plasticity, and self-renewal capacity, differentiation of tumor cells in solid tumors, including gliomas, can potentially promote tumor cell senescence and sensitize gliomas to immunotherapy, suggesting its multifaceted benefits from a therapeutic perspective[36-39].

Therapeutic differentiation of oligodendrocyte progenitor cells (OPCs) to become myelinating oligodendrocytes has been extensively pursued for treating multiple sclerosis (MS), a demyelinating disease that affects millions of patients worldwide. Several drugs have been shown to effectively differentiate OPCs to myelinating oligodendrocytes in various *in vivo* disease models[40-42]. Notably, the PN subtype GBMs display molecular signatures reminiscent of OPCs, both at the individual tumor level

and at the single cell level, suggesting their OPC origin and progenitor features[9,12]. We hypothesized that diminishing the progenitor features of these GBM cells via induction of differentiation can suppress their stemness and tumorigenicity. We identified clemastine, a low-toxicity, non-oncology drug for alleviating allergy symptoms with high potency in promoting OPC differentiation[40-42], as an agent that can be used to inhibit the propagation of BTIC cultures. Using BTIC cultures bearing *PDGFRA* amplification to represent PN subtype GBMs, we found that the tumor suppressive effects of clemastine were accompanied by diminished stemness of tumor cells and altered molecular signatures indicative of more differentiated states. Corroborating these findings, loss-of-function assays of putative pharmacological targets of clemastine identified Emopamil Binding Protein (EBP), a crucial enzyme in the cholesterol biosynthesis pathway, as an essential protein for maintaining BTIC proliferation and stemness. Finally, clemastine suppressed the *in vivo* tumorigenicity of a mouse glioma cell line resembling the PN subtype of GBMs. This study identifies new candidate proteins in GBM cells that can be therapeutically targeted (i.e., EBP), and suggests that clemastine and other agents capable of inducing OPC differentiation can be leveraged for attenuating the stemness/plasticity of GBM cells, particularly those bearing PN features. Our findings support the principle of repurposing non-oncology drugs for inducing differentiation and thus mitigating GBM stemness.

Results

Clemastine suppresses the propagation of patient-derived BTIC cultures

Several drugs with OPC-differentiating activity have been shown to effectively stimulate normal OPC differentiation and subsequent remyelination in multiple *in vivo* disease models[40-42]. These findings prompted us to test the effects of these drugs on GBM cells bearing OPC features. The PN subtype of GBM, typified by OPC-like transcriptomes, is characterized by IDH1 mutations or *PDGFRA* amplification, while *EGFR* amplification associates with the CL subtype[9]. Therefore, we first identified GBM lines with predominantly *EGFR* amplification (*EGFR*$^+$, representing CL GBMs), both *PDGFRA* and *EGFR* amplifications (in agreement with the heterogeneous nature of GBMs that are observed), as well as lines that bear predominantly *PDGFRA* amplification (*PDGFRA*$^+$, representing PN GBMs) (**Supplementary Fig. 1A**). We then cultured two *PDGFRA*$^+$ lines (BTIC#102 and BTIC#148, with ~25x and ~3x *PDGFRA* amplification, respectively) in serum-free neural stem cell medium to maintain their stemness properties as BTIC cultures, and determined the effects of a small panel of OPC-differentiating drugs on BTIC propagation. We found that all of these drugs suppressed the propagation of BTICs in a dose-dependent manner (**Supplementary Fig. 1B-C**). Among them, tamoxifen,

benztropine, and clemastine were previously found to promote OPC differentiation by affecting the cholesterol biosynthesis pathway[43]. Of note, clemastine is a safe, over-the-counter (OTC) allergy relief medicine that can cross the blood-brain barrier (BBB) and induce remyelination[40,41,44]. It has shown promising therapeutic benefits via differentiation induction in demyelinating models[40-42], and most remarkably, in clinical trials for MS patients[44,45]. These findings prompted us further to characterize the inhibitory effects of clemastine. We found that the effects of clemastine on BTICs were accompanied by cell morphology alterations (**Fig. 1A-B** and **Supplementary Fig. 2A-B**) and suppressed cell proliferation (**Fig. 1C** and **Supplementary Fig. 2C**). Notably, following 10-day clemastine pre-treatments, the antiproliferative effects of clemastine persisted even after clemastine was removed from the media (**Fig. 1D** and **Supplementary Fig. 2D**). Collectively, these results suggest that clemastine induced lasting alterations in *PDGFRA*$^+$ BTICs and suppressed the propagation of these tumor cells.

While we had focused on PN-like BTICs that are believed to serve broadly as progenitors of GBMs[16] and transition between one subtype to another (e.g., PN to MES GBMs)[14,15], the intratumoral heterogeneity of GBMs consisting of various subtypes[7-12] prompted us to examine the effects of clemastine in primary BTIC cultures resembling other subtypes. We used two primary *EGFR*$^+$ BTIC cultures (representing the CL subtype: BTIC#127 and BTIC#095) (**Supplementary Fig. 1A**) and two primary BTIC cultures that were shown to bear MES transcriptomic signatures (GSC-1123 and JK-046[46,47]) for this purpose. We found that BTIC cultures resembling the CL and MES subtypes were also susceptible to clemastine treatment, as indicated by reduced cell proliferation (**Fig. 1E**), suggesting that the anti-proliferative effects of this drug impact BTICs broadly and independent of tumor subtypes. Importantly, unlike the tumor cells tested, the proliferation of normal human astrocytes was not affected by the treatment (**Fig. 1F**). Collectively, these results implicate clemastine as a BTIC-suppressive drug and provide a basis for repurposing clemastine, and potentially other remyelinating agents, for targeting GBMs.

Clemastine attenuates the stemness and progenitor cell features of *PDGFRA*$^+$ BTICs

Clemastine has been shown to promote the differentiation of OPCs to mature oligodendrocytes in treating MS[43,48]. This prompted us to investigate whether the effects of clemastine on BTICs involved such a differentiation induction mechanism. We used *PDGFRA*$^+$ BTIC cultures as the prototypic models with the rationale that the OPC-like status of these tumor cells can facilitate assessing their progenitor versus differentiated states. We treated the *PDGFRA*$^+$ BTIC cultures with clemastine and evaluated the expression of key markers indicative of neural stem cell (NSC) and OPC properties. In agreement,

clemastine treatment resulted in decreased expression of marker genes for NSCs (*NES*[49], *SOX2*[50]), OPCs (*OLIG2*[51], *PDGFRA*[52], *CSPG4*[53]), and negative regulators of OPC differentiation (e.g., *NOTCH1*, *CSPG5*[54]) in the two *PDGFRA*$^+$ BTIC cultures (**Fig. 2A** and **Supplementary Fig. 3A**). Intriguingly, *MOG*, an oligodendrocyte maturation marker gene[55], displayed upregulated expression in clemastine-treated cells (**Fig. 2A**). The reduced expression of these molecular markers of NSCs and OPCs was confirmed at their protein levels by immunoblots (**Fig. 2B** and **Supplementary Fig. 3B**) and immunofluorescent staining (**Fig. 2C** and **Supplementary Fig. 3C**). To further investigate cell state changes following clemastine treatment, we utilized BTIC#102, the line with a high level of *PDGFRA* amplification and PDGFRA expression (i.e., more OPC-like), to facilitate studying the differentiating effects. The diminished progenitor states and potential differentiation of tumor cells were corroborated by the induction of GALC protein expression, another oligodendrocyte maturation marker[55], in parallel with the reduced level of PDGFRA protein (**Fig. 2D-E**). The increased presence of GALC$^+$ and reduced presence of *PDGFRA*$^+$ cells (**Fig. 2F**), together with the mutually exclusive staining pattern of these proteins (**Fig. 2G**), suggest these tumor cells indeed became more differentiated upon clemastine treatment.

The altered expression of marker genes associated with progenitor or differentiated cells prompted us to examine the changes in the global gene expression (mRNA-seq) of the two *PDGFRA*$^+$ BTIC cultures in response to clemastine. Consistent with our observations mentioned above, transcriptomic profiling from the mRNA-seq data revealed an overall downregulated expression of most dominant marker genes for OPCs[56] in response to clemastine treatment in both BTIC cultures (**Fig. 2H** and **Supplementary Fig. 3D**). mRNA-seq analyses also revealed upregulated expression of a fraction of marker genes for newly formed oligodendrocyte (NFO) and myelinating oligodendrocytes (MO)[56] in response to clemastine treatment (**Fig. 2I** and **Supplementary Fig. 3E**). Gene Set Enrichment Analysis (GSEA) confirmed the clemastine-induced downregulation of genes associated with OPCs (**Supplementary Fig. 3F-G**), and downregulation of genes in the protein translation machinery (**Supplementary Fig. 3H-I**), which serves a critical role in cancer cell stemness/plasticity and as a promising therapeutic target[57,58].

To assess the functional consequence of the altered gene expression profiles described above, we determined the effects of clemastine on the stem-like properties of BTICs as measured by their self-renewal capability[59,60], via the Extreme Limiting Dilution Assay (ELDA)[61]. We found that clemastine treatment diminished the self-renewal capability of BTICs (**Fig. 2J**). More notably, reminiscent of the lasting effects of clemastine on BTIC propagation, BTICs that were exposed to clemastine and then

maintained in clemastine-free media also displayed a diminished self-renewal capacity, suggesting a persistent effect of clemastine on BTIC stemness (**Fig. 2K**). Together with the altered gene expression profiles, these results suggest that clemastine attenuates the stemness/progenitor properties of BTICs by promoting differentiation.

EBP, a pharmacological target of clemastine, is essential for BTIC propagation

Pharmacologically, clemastine is known to act as an antagonist for histamine H1 receptor (H1R, encoded by *HRH1*) and muscarinic receptors (M1R-M5R, encoded by *CHRM1-CHRM5,* respectively)[62], and to target EBP, an enzyme in the cholesterol biosynthesis pathway. The well-established antagonist activity of clemastine against H1R and the inhibitory effects of M1R and M3R signaling on oligodendrocyte differentiation[63,64] prompted us to determine the expression profiles of these three receptor genes (*HRH1*, *CHRM1,* and *CHRM3*) in gliomas. We found that *HRH1* and *CHRM3* were expressed at higher levels in GBM (grade IV) in comparison to lower-grade gliomas (grade II and III), while *CHRM1* displayed the opposite trend (**Supplementary Fig. 4A**). This result led us to experimentally assess the roles of H1R and M3R in BTICs. First, two second-generation H1R-antihistamines, fexofenadine (Allegra) and cetirizine (Zyrtec)[65], were found to have no suppressive effects on BTICs, suggesting these cells were not affected by the H1R signaling blockade (**Supplementary Fig. 4B**). Furthermore, CRISPR/Cas9-mediated individual gene knockout of *HRH1* or *CHRM3* (**Supplementary Fig. 4C**) did not affect the propagation of BTICs or the susceptibility of BTICs to clemastine (**Supplementary Fig. 4D**). As the tumor-supporting roles of each gene may be affected by the variable genetic makeups specific for each tumor model, these results did not conclusively rule out the involvement of these receptors in mediating the effects of clemastine. Nevertheless, these findings led us to investigate other potential targets of clemastine. Interestingly, pharmacological inhibition of EBP has been shown to effectively induce the differentiation of OPCs to become oligodendrocytes[43,48], which prompted us to examine the roles of EBP in GBM (**Supplementary Fig. 5A**).

First, analysis of mRNA-seq data from The Cancer Genome Atlas (TCGA)[66] via the Gliovis data portal[67] revealed that, distinct from genes encoding other enzymes in the cholesterol biosynthesis pathway, EBP displayed upregulated expression in GBMs in comparison to non-tumor tissues as well as to lower grade gliomas (grade II and III) (**Supplementary Fig. 5B**). Notably, two additional properties distinguish EBP from other enzymes in the cholesterol biosynthesis pathway: EBP mutations have been linked to Conradi-Hünermann-Happle (CHH) syndrome[68], and it is known to be a protein target of numerous

structurally diverse pharmacological agents[69-71]. In fact, EBP is the common pharmacological target shared by seven out of the eight OPC-differentiating drugs included in our initial test[43,48,69,70] (**Supplementary Fig. 1B-C**). These unique features, together with the therapeutic potential of targeting EBP, led us further to assess the pathological functions of this protein in GBM.

We used the patient-derived BTIC cultures to determine the roles of EBP in GBM. Knockdown of EBP in BTICs resulted in significant suppression of BTIC propagation, which was accompanied by altered cell morphology (**Fig. 3A-B** and **Supplementary Fig. 6A-B**) and reduced expression levels of featured OPC marker genes, including *PDGFRA*, *CSPG4,* and *OLIG2* (**Supplementary Fig. 6C).** Conversely, echoing the finding from the loss-of-function assays, overexpression of exogenous EBP promoted BTIC propagation (**Fig. 3C** and **Supplementary Fig. 6D-E)**. Several pathogenic, missense mutations of EBP have been identified in CHH patients with various degrees of reduction in enzymatic activities[68,72,73]. We assessed if the enzymatic activity is required for the promoting effect of EBP by overexpressing three of the EBP mutants, EBP-E80K, EBP-R147H, EBP-W196S, or the wildtype EBP in BTIC#102 cells (**Supplementary Fig. 6F-G**). Of note, levels of these mutant EBP proteins were lower than the wildtype EBP protein (**Supplementary Fig. 6F-G**), likely due to their various stabilities. Nevertheless, among the three mutants, which had comparable expression levels, EBP-E80K, the mutant known to have minimal enzymatic activity retained, had lower potency in promoting the growth of the GBM culture compared to EBP-R147H, a mutant that possesses partial enzymatic activity[68,74] (**Fig. 3D**). Taken together, these results suggest that EBP is essential for BTIC propagation and that the GBM-promoting effects of EBP likely require its enzymatic activity.

Several additional lines of evidence corroborate the findings mentioned above and support that suppressing EBP partially mediates the effects of clemastine on BTICs. First, the addition of exogenous cholesterol to the culture media partially rescued the suppressive effects of clemastine on BTIC propagation (**Fig. 3E** and **Supplementary Fig. 6H**). Furthermore, the presence of the immediate metabolic product of EBP, lathosterol, also partially countered the suppressive effects of clemastine on BTIC propagation. Of note, the addition of exogenous lathosterol alone at a higher dose moderately suppressed tumor cell propagation (**Fig. 3F** and **Supplementary Fig. 6I**), suggesting that an optimal dose of this metabolite and maintaining the homeostasis of the cholesterol pathway are essential for the optimal growth of tumor cells. Finally, we found that stable overexpression of EBP in primary BTICs conferred partial protection from clemastine (**Fig. 3G**). Collectively, the above results suggest that BTIC propagation depends on EBP, a pharmacological target of clemastine, and the homeostasis of the

cholesterol pathway, and provide a potential mechanism underlying the suppressive effects of clemastine.

Clemastine suppresses tumorigenicity in a mouse glioma model representative of PN GBMs

We postulated that a GBM model with a better-defined genetic makeup could provide advantages to further characterize the tumor suppressive effects of clemastine. For this purpose, we generated mouse NSC lines from a conditional *Trp53* knockout mouse model previously described[75,76]. NSCs derived from these models underwent adenoviral Cre-recombinase mediated *Trp53* deletion followed by overexpression of exogenous *Pdgfb*, an oncogene that has been shown to induce gliomas that resemble PN GBMs[77-81]. The genetically-modified NSC lines were then orthotopically implanted into mice to generate PDGFB-driven, aggressive glioma tumors with high penetrance and short latency (**Supplementary Fig. 7A**). Gene expression profiling (mRNA-seq) of the tumor tissues and subtyping analysis utilizing the previously defined subtype-specific gene signatures[81] confirmed their predominant PN features, and the detectable expression of genes associated with other subtypes recapitulated the heterogeneous nature of GBMs (**Supplementary Fig. 7B**). A glioma cell line derived from these tumors (named C266) was used to investigate its dependency on EBP protein and susceptibility to clemastine, benztropine, and a small-molecule drug (CW3388) known to inhibit mouse EBP[48]. Results from these experiments using the mouse glioma cell line corroborate findings from human BTICs, as elaborated in the following:

First, knockdown of *Ebp* resulted in attenuated growth (**Fig. 4A** and **Supplementary Fig. 7C-D**) and reduced self-renewal capacity (**Fig. 4B**) of the mouse glioma cell line. Second, treating C266 cells with CW3388 resulted in decreased cell proliferation (**Fig. 4C**). Similarly, the mouse glioma line also displayed suppressed propagation in response to clemastine and benztropine treatment, recapitulating the findings from human BTICs (**Fig. 4D** and **Supplementary Fig. 7E**). Third, echoing the effect of EBP's abundance on human BTIC's susceptibility to clemastine, *Ebp* knockdown rendered mouse glioma cells more sensitive to clemastine and CW3388 (**Fig. 4E** and **Supplementary Fig. 7F**), suggesting that clemastine acted in the same manner as CW3388. Taking advantage of the aggressive nature of this tumor cell line in orthotopic mouse models, we tested the suppressive effects of clemastine *in vivo*. We found that the clemastine treatment led to a delayed progression of tumors *in vivo*, as evidenced by the slower tumor progression (**Fig. 4F**), and a small subset of mice (20%) that had extended survival with measurable tumor signal two months post-implantation (at which points mice were terminated) (**Fig. 4G**). The reasons for this delayed yet extended benefit remained unclear,

and we speculate that the treatment likely altered the progenitor properties of tumor cells instead of acutely killing them *in vivo*. Finally, we noted that mice subjected to this treatment regimen displayed no different body weight compared to the control mice, suggesting its minimal toxicity (**Fig. 4H).**

Clemastine treatment broadly alters multiple signaling pathways in glioma cells

While clemastine has multiple pharmacological targets and its effects on cell signaling pathways are expected to be broad and dependent on the genetic composition of GBM cells, we postulated that identifying pathways that were perturbed by clemastine and/or CW3388 in the mouse glioma cell line could provide additional insights into the molecular mechanisms of clemastine. Therefore, we performed mRNA-seq to identify differentially expressed genes in clemastine or CW3388-treated C266 cells (**Supplementary Table 1**). Several findings were noted. First, among the 10,292 genes identified, 18.3% (1,888 genes) of them were affected by clemastine. In comparison, among those genes affected by CW3388 (2,759 genes), the number increased to 45.7% (1,261 genes), suggesting genes affected by clemastine were enriched in the CW3388-responsive gene set ($p < 0.0001$). Additionally, among genes affected by both agents, an overwhelming majority of them (1,210 out of 1,261; 96.0%) displayed the same directional changes (i.e., up- or down-regulation) in response to both agents, further supporting that clemastine and CW3388 act on overlapping genes/pathways in the tumor cells. Second, GSEA for differentially expressed genes presented a positive enrichment of genes corresponding to oligodendrocytes in response to either clemastine or CW3388, in agreement with their expected effects on tumor cell's progenitor identity (**Supplementary Fig. 8**). Third, in clemastine-treated cells, KEGG pathway analysis identified pathways in cancers, metabolism, Wnt, and PI3K-AKT signaling pathways (**Supplementary Table 2**). Notably, similar analyses comparing the CW3388-treated versus the vehicle-treated cells identified an overlapping set of KEGG pathways (**Supplementary Table 2**). Panther pathway analysis pinpointed smaller numbers of altered pathways using the same criteria (FDR $\leqq 0.05$), and revealed that a majority of the CW3388-affected pathways were also identified as being perturbed by clemastine (**Supplementary Table 2**). These results suggest that the impacts of clemastine overlap with and exceed those of CW3388, in agreement with its expected pharmacological activity targeting multiple proteins, including EBP.

We employed signaling pathway impact analysis, which incorporates over-representation analysis and functional class scoring and has been shown to have superior specificity and sensitivity in identifying altered pathways[82], to analyze differentially expressed genes of patient-derived BTIC cultures in response to clemastine (**Supplementary Table 3**). This analysis identified numerous KEGG pathways

that were affected in the BTIC cultures (196 and 154 were identified in BTIC#102 and BTIC#148, respectively). Although the pathways varied between these models, likely due to the various genetic background and different basal gene expressions in matched control cells, 142 common pathways were identified in both BTIC cultures, including cell adhesion, cholesterol metabolism, and the PI3K-AKT signaling pathway (**Supplementary Table 4**). Collectively, these pathway analyses suggest the pleiotropic consequences of clemastine treatment at the molecular level, and also highlight the substantial alterations in cellular processes and oncogenic signaling pathways in tumor cells, including cell metabolism, the Wnt signaling pathway, and the PI3K-AKT pathway. While such assays could not distinguish pathway alterations that contributed to the tumor suppression from those that resulted from cell adaptation/population evolution, these results resonate with our findings in the mouse glioma cell line, and yield additional evidence that supports the tumor suppressive effects of clemastine.

Discussion

BTICs are key drivers of GBM's resistance to treatments, progression, and recurrence. In this study, we showed that clemastine, an over-the-counter drug used for alleviating allergies, suppresses the propagation of patient-derived BTICs bearing *PDGFRA* amplification (as a surrogate representing the PN GBMs), as well as those resembling CL or MES subtypes. We further used the PN/OPC-like BTICs to demonstrate that this drug attenuates the stemness/progenitor features of tumor cells. Finally, we showed that pharmacological targets of clemastine, as highlighted by EBP, are essential for the proliferation of these tumor cells.

The suppressive effects of clemastine on the BTICs described in the current study corroborate the findings from previous research on clemastine. First, it was shown that clemastine could compromise the lysosomal membrane integrity in glioma cells to suppress glioma cell tumorigenicity[83]. This study aligns with our findings in supporting that this drug can act on multiple pathways and cellular processes to exert tumor suppressive effects, and provide a foundation for investigating the detailed mechanisms in further studies. Second, induction of normal OPC differentiation into myelinating oligodendrocytes by clemastine has yielded promising therapeutic benefits in clinical trials in MS patients, validating the *in vivo* therapeutic efficacy of clemastine and its permeability across the blood-brain barrier[44,45]. We note that, unlike in normal cells, genetic and epigenetic alterations in tumor cells most likely preclude the possibility of accomplishing terminal differentiation in the latter. Nevertheless, the suppressive effects of clemastine on GBM stemness could provide therapeutic benefits, particularly when combined with therapeutics such as those that target other subtypes of GBMs. This strategy can potentially mitigate

the emergence or selection of the evolved populations, such as those driven by EGFR oncogenic signaling[15].

Loss-of-function of EBP, a protein that is pharmacologically inhibited by clemastine[43,48], recapitulated the suppressive effects of clemastine, as indicated by both attenuated BTIC stemness and the accompanied differential gene expression. Taken together with the dependency of BTICs on EBP, our study implicates sterol metabolism in GBM stemness maintenance. Prior studies support that inhibitors for certain enzymes in the cholesterol biosynthesis pathway, including EBP, can promote remyelination, linking this pathway and the involved intermediate metabolites to promoting normal OPC differentiation[43,48]. In addition, lipid biosynthesis and the cholesterol pathway have been demonstrated to be promising therapeutic targets for treating GBMs[84-88]. For instance, intermediate metabolites in the cholesterol pathway have been found to exert the tumor suppressive effects via activating endogenous liver X receptors (LXRs) in GBM[84,87] and another type of brain tumor, diffuse intrinsic pontine glioma (DIPG)[89]. Thus, our results are consistent with previous literature that highlights tumor cell's dependency on the homeostasis of the cholesterol pathway.

Two outstanding issues remain to be further investigated. First, although EBP inhibition likely contributed to the suppressive effects of clemastine, the underlying mechanism of clemastine-mediated EBP inhibition remains to be studied. This issue is complicated by EBP's unique multi-drug binding capacity and the possibility that EBP lowers the intracellular concentration of drugs that inhibit its activity[74,90,91], which provide an alternative explanation for the findings that knockdown of EBP conferred tumor cell's sensitivity (and vice versa) to its inhibitors (such as clemastine and CW3388). Second, illustrating the molecular mechanisms of the tumor suppressive effects of EBP inhibition will be critical for assessing the potential of this enzyme as a therapeutic target. It is possible that EBP inhibition alters the intermediate metabolite composition in tumor cells (cell-autonomous) and/or in the tumor microenvironments (e.g., non-tumor cells). Alternatively, the upregulated expression of EBP in GBMs, a trend that is opposite to several other enzymes in the cholesterol biosynthesis pathway, as well as the complicated pharmacological property of this protein[69,70], raise the possibility that its inhibition affects cellular processes other than simply disrupting the biosynthesis pathway of cholesterol.

In summary, findings from this study support the feasibility of inducing differentiation for targeting the stemness of gliomas bearing OPC features, which include not only PN-like GBM, but also oligodendroglioma and DIPG[92,93]. We provide evidence to support exploiting clemastine, or other non-

oncology, low-toxicity drugs with similar activity in targeting EBP and/or inducing differentiation[69,70,94], for targeting GBM stemness. In addition, the study also nominates EBP as a therapeutic target in GBM. During the preparation of this manuscript, the FDA has granted orphan drug designation (ODD) for DSP-0390, a newly developed inhibitor of EBP (https://www.targetedonc.com/view/fda-grants-orphan-drug-designation-to-dsp-0390-in-brain-cancer), for which a phase I clinical trial for treating recurrent high-grade gliomas has been initiated (NCT05023551)[95]. The results presented in this study provide evidence to support such actions. We propose that further studies assessing the underlying pathogenic mechanism of EBP, and the therapeutic efficacy of EBP inhibitors on various subtypes of GBM cells combination with other treatment approaches, are warranted.

Materials and Methods

Cell lines Primary GBM cultures (BTIC#102, BTIC#148, BTIC#127, and BTIC#095) were derived with consent from tumor tissues of patients at the Duke Brain Tumor Center. GBM cultures GSC-1123 and JK-046 were previously described[46,47]. These GBM cell lines were maintained as BTICs in human neural stem cell (NSC) media containing NeuroCult NS-A basal medium (human, STEMCELL Technologies, #05750), supplemented NeuroCult NS-A proliferation kit (human, STEMCELL Technologies, #05751), human recombinant EGF (20 ng/mL, STEMCELL Technologies, #78006.2), human recombinant FGF (10 ng/mL, STEMCELL, #78134.1), and heparin sodium salt (2 µg/mL, MilliporeSigma, #H3149-100KU). The mouse glioma cell line (C266-6-IC-12/12, simplified as “C266”), established from tumors originating from *Trp53*$^{-/-}$ mouse NSC transduced with retrovirus-*Pdgfb*, was cultured in standard mouse NSC media containing NeuroCult basal medium (mouse & rat, STEMCELL Technologies, #05700) supplemented with NeuroCult proliferation kit (mouse & rat, STEMCELL Technologies, #05702), human recombinant EGF (20 ng/mL, STEMCELL Technologies, #78006.2), human recombinant FGF (10 ng/mL, STEMCELL, #78134.1), and heparin sodium salt (2 µg/mL, MilliporeSigma, #H3149-100KU). Normal human astrocytes (Lonza, #CL-2693-FV) were purchased from the Duke Cell Culture Facility and cultured in growth media containing MCDB 131 medium (no glutamine, Thermo Fisher Scientific, #10372019) supplemented with ascorbic acid (75 µg/mL, Lonza, #CC-4398), human recombinant insulin (20 µg/mL, Lonza, #BE03-033E20), human recombinant EGF (2 ng/mL, STEMCELL Technologies, #78006.2), antibiotic-antimycotic (1X, Thermo Fisher Scientific, #15240062), fetal bovine serum (3%, Cytiva, #SH30071.03T), and GlutaMAX supplement (2 mM, Thermo Fisher Scientific, #35050061). Cells were grown as suspension or on laminin-coated plates at 37^{o}C and 5% CO_2, and experiments were performed within 30 passages after cells were thawed.

shRNA-mediated gene knockdown cells were generated by transducing cell lines of interest with lentivirus containing pLKO.1 vector with non-targeting control shRNA or shRNA sequences targeting either *EBP* or *CHRM1* (purchased from Duke Functional Genomics Shared Resource) at an MOI of 1 or 3. CRISPR/Cas9-mediated gene knockout cells were generated by transducing BTIC#102 cells with *HRH1* and *CHRM3* CRISPR/Cas9 knockout lentivirus. Luciferase-expressing cells were generated by transducing C266 cells with CMV-Firefly luciferase lentivirus (Cellomics Technology, #PLV-10003-50) at an MOI of 1. All transduction reactions were supplemented with 6 μg/mL polybrene (MilliporeSigma, #TR-1003). Virus-containing media were removed after 24 hours of transduction and replaced with appropriate media. Transduced cells were selected with puromycin (MilliporeSigma, #P8833) at 1 μg/mL for 5 days and subsequently maintained in 0.3 μg/mL puromycin (except in proliferation assays, in which cells were cultured in puromycin-free media).

Chemicals, other reagents, and plasmids Chemicals and other molecular biology reagents used are listed in the Supplementary Materials. Briefly, stock solutions of all remyelinating agents were prepared in dimethyl sulfoxide (DMSO), with clemastine and benztropine prepared at 10 mM and other remyelinating agents at 20 mM, and stored at -20°C. 200 μM working solutions were then prepared by diluting the 10 mM stock solutions with human or mouse standard NSC media and stored at -20°C. CW3388 stock solutions were prepared in dimethyl sulfoxide (DMSO) at 2 mM and stored at 4°C. Lathosterol stock solutions were prepared in ethanol at 12.5 mM, water-soluble cholesterol stock solutions were prepared in PBS at 4 mM, and stock solutions of H1R inhibitors were prepared in DMSO at 10 mM.

The pcDNA3.1 V5-His A plasmid was a kind gift from Dr. Vidyalakshmi Chandramohan, and the pcDNA3.1+-C-(K)-DYK plasmid expressing Flag-EBP was purchased from GenScript (#OHu18817). Primers for site-directed mutagenesis of the *EBP* gene were designed using the QuikChange Primer Design Program (https://www.agilent.com/store/primerDesignProgram.jsp?_requestid=1072141) and listed in the Supplementary Materials. Three EBP mutant constructs (E80K, R147H, W196S) were constructed from pcDNA3.1+-C-(K)-DYK-*EBP* plasmids using the QuikChange Lightning Multi Site-Directed Mutagenesis Kit (Agilent Technologies, #210519) following the manufacturer's protocol. All plasmid sequences were verified by Sanger sequencing provided by Genewiz.

For CRISPR/Cas9-mediated gene knockout plasmids, single guide RNA (sgRNA) sequences targeting the exons of *HRH1* and *CHRM3* genes were designed using the CRISPOR web tool (http://crispor.tefor.net/) and listed in Supplementary Materials. *HRH1* and *CHRM3* CRISPR/Cas9

knockout plasmids were constructed from LentiCRISPRv2E plasmids by first phosphorylating and annealing paired sgRNAs with 10X T4 ligation buffer (New England Biolabs, #B0202S) and T4 polynucleotide kinase (New England Biolabs, #M0201S), and then ligating annealed sgRNAs and pre-digested and purified LentiCRISPRv2E vector with Quick Ligation Kit (New England Biolabs, #M2200S). Plasmids were verified to contain expected sgRNA sequences by colony PCR (using LKO.1 5' and pLentiCRISPR-R1 primers) and/or Sanger sequencing (Genewiz, using T7 primers) using PCR primers listed in Supplementary Materials. *HRH1* and *CHRM3* CRISPR/Cas9 knockout lentivirus was prepared by transfecting HEK293FT cells with Lipofectamine 3000 transfection reagent (Thermo Fisher Scientific, #L3000015) and plasmids including pLP1, pLP2, pLP/VSVG, and two LentiCRISPRv2E plasmids containing different sgRNA sequences targeting the same gene (*HRH1* or *CHRM3*). Control lentivirus was prepared parallelly using LentiCRISPRv2E plasmids containing control sgRNA sequences.

Plasmid electroporation Cells were transfected with pcDNA3.1 V5-His A, pcDNA3.1+-C-(K)-DYK plasmids encoding either wild-type EBP or one of the three mutant EBPs (E80K, R147H, W196S), EGFP-hGal3, or PM-GFP plasmids using Neon Transfection System 10 µL Kit (Thermo Fisher Scientific, #MPK1025) following the manufacturer's protocol. In brief, cells were prepared and resuspended in buffer R at a concentration of 100,000 cells/10 µL buffer R. 10 µL of cell suspension was then added to each plasmid solution containing 0.5 µg or 1 µg of plasmid DNA. The cell-plasmid DNA mixtures were then subjected to electroporation using the Neon Transfection System and transferred into laminin-coated 24 well plates containing 500 µL of prewarmed standard NSC media in each well. Transfected cells were selected with G418 sulfate (ThermoFisher Scientific, #10131035) at 250 µg/mL for 5 days and subsequently maintained in 100 µg/mL G418 sulfate (except in proliferation assays, in which cells were cultured in G418-free media).

BTIC proliferation assay, cell cycle analysis, and ELDA Cell proliferation assays were performed by seeding the cell lines of interest in their respective media with either vehicle or drugs of interest at a density of 1500-3000 cells/well and a final volume of 200 µL/well in laminin-coated 96-well clear flat bottom plates. Cells were incubated overnight in a humidified incubator at 37°C and 5% CO_2, and then placed in the IncuCyte S3 Live-cell analysis system and scanned every 4 hours using the whole well, phase contrast acquisition mode (4X objective) for 7-14 days. Phase area confluence was obtained and calculated by the IncuCyte system, normalized to day 0 to generate relative phase object area (fold change), and then presented as mean ± S.E.M.. For cell cycle analyses, cells were re-suspended in 500 µL of ice-cold PBS and triturated to obtain a single cell suspension. Ethanol fixation was performed

by first adding 3 mL of ice-cold 70% ethanol to the cell suspension in a drop-wise manner while vortexing, and then incubating the cell-ethanol mix at -20°C for 1 hour. The fixed cells were washed with ice-cold PBS three times, resuspended in 500 µL FxCycle™ PI/RNase Staining Solution (ThermoFisher Scientific, #F10797), and incubated at room temperature for 30 minutes while protected from light. Samples were analyzed with BD Fortessa X-20 with the BD FACSDiVa software (BD Biosciences, San Jose, CA, USA). ELDAs with or without pretreatment were performed as previously described[96,97].

***In vivo* drug treatment** Orthotopic intracranial tumor implantation and *in vivo* bioluminescent imaging were performed as previously described[96,97]. Briefly, C266mouse glioma cells (~100,000 cells, expressing luciferase) were mixed 1:3 with methylcellulose and injected into the right caudate nucleus of female athymic nude mice (Jackson Labs, Bar Harbor, ME, USA; strain #:007850), and tumor treatment was initiated 4 days post-implantation. Mice were treated with vehicle control or clemastine at 30 mg/kg via intraperitoneal (i.p.) injection daily for five days per week (15% DMSO in PBS was used as the vehicle control). *In vivo* drug response was monitored weekly by bioluminescent imaging of mice and analyzed using Living Image software (PerkinElmer, Waltham, MA, USA). Mouse body weight was documented at least every two days. All animal experiments were performed in accordance with protocols approved by the Duke University Institutional Animal Care and Use Committee (IACUC), Protocol #A133-19-06 (approved 27 June 2019).

Reverse transcription and real-time quantitative PCR (RT-qPCR) BTIC cultures were plated at a density of 80,000-120,000 cells/well in laminin-coated 6 well plates in standard NSC media and incubated overnight to allow them to adhere. Next day, cells were treated with either vehicle or drugs. Cells were passaged every 5-7 days into fresh media containing respective treatments, and then harvested on day 9-14 for total RNA extraction using the Quick-RNA Miniprep kit (Genesee Scientific, #11-328) following the manufacturer's protocol. The concentration and the A260/A280 ratio of each RNA sample were measured with Nanodrop Lite Spectrophotometer (Thermo Fisher Scientific, #ND-LITE). RNA samples with concentration > 30 ng/µL and A260/280 ≧ 2.0 were diluted to the same concentration with DNase/RNase-free distilled water, and then the same amount of RNA/H_2O mix (containing 1 µg of total RNA) from each sample was reverse-transcribed to cDNA using the EcoDry cDNA synthesis kit (Takara Bio, #639548) following the manufacturer's protocol. Real-time quantitative PCR was performed using gene-specific qPCR primers listed in Supplementary Materials and the KAPA SYBR Fast qPCR Master Mix (2X) kit (Kapa Biosystems, #KK4602), and ran on CFX96 Real-Time PCR Detection System (BIO-RAD, Hercules, CA, USA). The results were analyzed using the CFX

Maestro Software (BIO-RAD, Hercules, CA, USA). The housekeeping genes *ACTB*, *B2M*, and *GAPDH* were used as internal controls for gene expression normalization.

Protein extraction and immunoblotting Total cellular protein was extracted from cell pellets using 1% SDS lysis buffer. Briefly, frozen cell pellets were resuspended with 80-120 µL 95°C preheated SDS lysis buffer (1% SDS, 50 mM NaF, 1 mM Na_3VO_4 in PBS, pH 7.4) and triturated until the suspensions were less gluey. The cell suspensions were then sonicated with Bioruptor Standard (Diagenode, #UCD-200) for 5 minutes at high intensity to achieve complete cell lysis, and heated at 95°C for 5 minutes. Cell lysates were centrifuged to remove residual cell debris, and supernatants, the protein extracts, were collected into new Eppendorf tubes. Protein concentrations were determined using the Pierce BCA Protein Assay kit (Thermo Fisher Scientific, #23225) following the manufacturer's protocol. The residual protein extracts were mixed with 4X Laemmli sample buffer (BIO-RAD, #1610747) at a ratio of 1:3, heated at 95°C for 5 minutes, and cool on ice for 5 minutes. The protein extracts with sample buffer were stored at -20°C or used immediately for gel electrophoresis. 10-15 µg of protein samples and 3-5 µL of Precision Plus Protein Dual Color Standards (BIO-RAD, #1610374) were loaded in NuPAGE 4-12% Bis-Tris protein gels (Thermo Fisher Scientific, #NP0321BOX, NP0322BOX, NP0335BOX, NP0336BOX) and ran in NuPAGE MOPS SDS Running Buffer (Thermo Fisher Scientific, #NP0001) supplemented with 500 µL of NuPAGE Antioxidant (Thermo Fisher Scientific, #NP0005). After gel electrophoresis, proteins were transferred from gels to nitrocellulose membranes (BIO-RAD, #1620115) by semi-dry transfer methods using the Trans-Blot Turbo Transfer System (BIO-RAD, #1704150). The membranes were then blocked with 5% non-fat dry milk (Genesee Scientific, #20-241) in TBST (0.1% Tween 20 in TBS) for 1 hour at room temperature, and incubated overnight at 4°C with primary antibodies diluted in antibody dilution buffer (5% BSA, 0.02% NaN_3 in TBST) according to the manufacturer's suggested dilutions (detailed information for antibodies and their dilutions were listed in Supplementary Materials). Next day, the membranes were incubated with appropriate horseradish peroxidase-conjugated secondary antibodies (Cell Signaling Technology, anti-rabbit IgG, #7074S; anti-mouse IgG, #7076S) diluted in TBST for 1 hour at room temperature. Then, the chemiluminescent signals were enhanced by incubating the membranes with SuperSignal West Pico PLUS Chemiluminescent Substrate (Thermo Fisher Scientific, #34580) following the manufacturer's protocol. The membranes were imaged with ChemiDoc MP System (BIO-RAD, #1708280) and analyzed with Image Lab Software (BIO-RAD, Hercules, CA, USA). To reprobe the membranes, membranes were stripped using Restore Western Blot Stripping Buffer (Thermo Fisher Scientific, #21059) and incubated with other primary antibodies following the manufacturer's protocol.

Immunofluorescence staining Cells were plated in laminin-coated 6 well plates and treated with either vehicle or clemastine (4 μM) as previously described. After 13-26 days of treatment (noted in the figure legends), the cells were plated on laminin-coated Nunc Lab-Tek II 2-well chamber slides (Thermo Fisher Scientific, #154461) and grown until they reached 80%-90% confluence. Cells were washed with PBS, fixed in 10% Neutral buffered formalin (VWR, #89370-094) or 4% formaldehyde (1:4 diluted from 16% formaldehyde with PBS) at room temperature for 15 minutes, and permeabilized with 0.1% saponin (MilliporeSigma, #84510, only in samples stained for GALC) or 0.3% Triton X-100 (Fluka, #93443) for 10 or 15 minutes, respectively. Slides with fixed and permeabilized cells were blocked with blocking buffer (1% BSA, 0.1% saponin or 0.2% Triton X-100, 10% goat serum in PBS) at room temperature for 1 hour, and then incubated with primary antibodies (detailed information of antibodies are listed in Supplementary Materials) diluted in antibody dilution buffer (1% BSA, 0.1% saponin or 0.2% Triton X-100 in PBS) at 4°C overnight. Next day, slides were washed three times with 0.1% saponin or 0.2% Triton X-100 in PBS, and incubated with appropriate secondary antibodies (anti-rabbit Alexa 594, #A-11037; anti-rabbit Alex 647, #A-21245; anti-mouse Alexa 488, #A-11029) 1:500 diluted in antibody dilution buffer at room temperature for 1 hour. Cells were stained with 1 μg/mL DAPI (MilliporeSigma, #D9542) before the slides were mounted with ProLong Gold Antifade Mountant (Thermo Fisher Scientific, #P36394) or SlowFade Diamond Antifade Mountant (Thermo Fisher Scientific, #S36972) following the manufacturer's protocol. The slides were imaged with Zeiss Axio Imager Z2 Upright Microscope and analyzed using the Zeiss Zen 3.5 (blue edition) software (Carl Zeiss Microscopy GmbH, Oberkochen, Germany).

Images from PDGFRA and GALC immunofluorescence staining of the vehicle or clemastine-treated BTIC#102 cells were analyzed using the CellProfiler software (version 4.2.1, Broad Institute, Cambridge, MA, USA)[98]. For quantification of mean fluorescence intensity of PDGFRA and GALC, "Cell" objects were first identified using DAPI signal as nuclear regions and PDGFRA/GALC signal to outline cell borders. The mean fluorescence intensity of PDGFRA and GALC per "Cell" object was measured, and the mean of mean fluorescence intensity per "Cell" object per field of view was then calculated. For quantification of percent positivity of PDGFRA and GALC, $PDGFRA^+$ and $GALC^+$ "Cell" objects were first identified using the mean fluorescence intensity per "Cell" object as thresholds, which were set using isotype-stained images as negative controls. The percentage of PDGFRA and GALC positive cells were then calculated as $\frac{\text{number of positive Cell object}}{\text{total number of Cell Object}}$ per field of view. To quantify the frequency distribution of $PDGFRA^+$ and/or $GALC^+$ cells, GALC positivity was determined in every $PDGFRA^-$ and $PDGFRA^+$ cell from all fields of view regardless of treatment status, and the contingency table was generated based on the calculated frequency distribution.

RNA-seq data and pathway analysis Next generation sequencing for mRNA-seq, including library construction and sequencing, was provided by Novogene Corporation Inc. (Sacramento, CA, USA). NovaSeq 6000 was used for PE150 sequencing. mRNA-seq data were analyzed using the Galaxy web platform via the public server at usegalaxy.org[99]. The workflow of RNA-seq analysis was adapted from a previously described procedure[100]. Briefly, raw data were trimmed by Trim Galore, aligned by Hisat2, re-assembled by StringTie, and differentially expressed genes (DEGs) were analyzed by Deseq2. All parameters were set at default. For pathway enrichment analysis, differentially expressed genes (DEGs, sorted by adjusted p-value < 0.05) were imported into ShinyGO[101] (http://bioinformatics.sdstate.edu/go/). For pathway analysis, KEGG and Panther pathways were used, and genes with adjusted p-value > 0 were input as the background gene list. For GSEA, all genes or genes with FDR ≦ 0.25 from human or mouse mRNA-seq data, respectively, were ranked by fold change and subjected to GSEA preranked analyses following the established protocol[102] using the GSEA software (version 4.1.0, Broad Institute, Cambridge, MA, USA). For pathway impact (two-evidence) analysis, all genes with adjusted p-values ≦ 0.05 were selected and subjected to analysis using ROntoTools[82], and pathways were ranked by combined FDR p-value (pComb.fdr).

Statistical Analysis All *in vitro* proliferation assays, cell cycle analyses, ELDA, quantitative RT-PCR, immunoblotting, immunofluorescence staining, and *in vivo* clemastine treatment experiments were repeated in at least two independent experiments. The number of independent samples was noted in the figure legends. Data were presented as mean ± standard error of the mean (S.E.M.) except for gene expression data, which were presented as geometric mean ± geometric standard deviation (S.D.), and ELDA data, which were shown as trend lines ± two-sided 95% confidence intervals. Mean values between two groups were compared by student t-tests (with Welch's correction when variances were deemed significantly different by F tests) or non-parametric Mann-Whitney tests. Mean values between 3 or more groups were compared by one-way or two-way ANOVA followed by Dunnett's or Tukey's multiple comparisons tests, respectively. Mean values between two or multiple groups over time were compared to the control group by two-way repeated measures ANOVA followed by Sidak's or Dunnett's multiple comparisons tests, respectively. Mean values of multiples groups were compared between all possible group pairings by two-way repeated measures ANOVA followed by Tukey's multiple comparisons tests. Geometric mean values of gene expression fold change were $\log_2$-transformed and analyzed by one-sample t-tests compared to zero. Survival analyses were performed using Log-rank (Mantel-Cox) tests. Contingency tables were analyzed using one-sided chi-square tests. All tests were two-sided if not otherwise specified and deemed statistically significant when p-values < 0.05. Normality

was tested before conducting any parametric test using Shapiro-Wilk normality tests. For proliferation assays, significance was calculated using the data from the last timepoints unless stated otherwise. All statistical analyses were performed using GraphPad Prism software (version 9.3.1, San Diego, CA, USA) except for ELDA (analyzed by ELDA online software: https://bioinf.wehi.edu.au/software/elda), Gliovis gene expression data (analyzed by Gliovis portal: http://gliovis.bioinfo.cnio.es/), RNA-seq, GSEA, and pathway analyses.

Code and Data availability statement All codes and data use will be available upon request. The data for RNA-seq were deposited with assigned GEO accession numbers GSE186319 and GSE186392.

Conflict of interest The authors declare no conflict of interest.

Acknowledgment We thank the Functional Genomics Core facility, the Duke Cancer Institute Flow Cytometry core facility, Duke Light Microscopy Core Facility, and The Cancer Center Isolation Facility (CCIF/DCI) for support of this study. We thank Dr. Vidyalakshmi Chandramohan for help with the construction of the EBP overexpression plasmids. This work was supported by the Preston Robert Tisch Brain Tumor Center and the Department of Pathology at Duke, the National Institute of Neurological Disorders and Stroke (NINDS) at the National Institutes of Health (NIH) (NS101074), a research grant from the American Brain Tumor Association (DG1900020), pilot research grants from Duke Cancer Institute as part of the NIH National Cancer Institute P30 Cancer Center Support Grant (CA014236), United States Army Medical Research Acquisition Activity W81XWH-22-1-0374 (to XS), and NIH NS115403, NS122375, NS126810, NS125318 (to SYC).

Author contributions Conception and design: MS, RY, YH; Methodology development: MS, RY, XS, BH, CJP, LHC, PKG, STK; Data acquisition: RY, MS, HL, WW, NR, KR, CJP; Data analysis and interpretation: MS, RY, CJP, YH; Writing, reviewing, and revision of the manuscript: MS, RY, CJP, DMA, YH, SYC, XS, BH**;** Administrative, technical, or material support: SYC, XS, BH, DDB, DMA, CJP, YH**;** Study supervision: YH.

References

1 Galli, R. *et al.* Isolation and characterization of tumorigenic, stem-like neural precursors from human glioblastoma. *Cancer Res* **64**, 7011-7021 (2004). https://doi.org:10.1158/0008-5472.CAN-04-1364

2 Ignatova, T. N. *et al.* Human cortical glial tumors contain neural stem-like cells expressing astroglial and neuronal markers in vitro. *Glia* **39**, 193-206 (2002). https://doi.org:10.1002/glia.10094
3 Singh, S. K. *et al.* Identification of a cancer stem cell in human brain tumors. *Cancer Res* **63**, 5821-5828 (2003).
4 Singh, S. K. *et al.* Identification of human brain tumour initiating cells. *Nature* **432**, 396-401 (2004). https://doi.org:10.1038/nature03128
5 Hemmati, H. D. *et al.* Cancerous stem cells can arise from pediatric brain tumors. *Proceedings of the National Academy of Sciences of the United States of America* **100**, 15178-15183 (2003). https://doi.org:10.1073/pnas.2036535100
6 Bao, S. *et al.* Glioma stem cells promote radioresistance by preferential activation of the DNA damage response. *Nature* **444**, 756-760 (2006). https://doi.org:10.1038/nature05236
7 Brennan, C. *et al.* Glioblastoma subclasses can be defined by activity among signal transduction pathways and associated genomic alterations. *PloS one* **4**, e7752 (2009). https://doi.org:10.1371/journal.pone.0007752
8 Patel, A. P. *et al.* Single-cell RNA-seq highlights intratumoral heterogeneity in primary glioblastoma. *Science* **344**, 1396-1401 (2014). https://doi.org:10.1126/science.1254257
9 Verhaak, R. G. *et al.* Integrated genomic analysis identifies clinically relevant subtypes of glioblastoma characterized by abnormalities in PDGFRA, IDH1, EGFR, and NF1. *Cancer cell* **17**, 98-110 (2010). https://doi.org:10.1016/j.ccr.2009.12.020
10 Phillips, H. S. *et al.* Molecular subclasses of high-grade glioma predict prognosis, delineate a pattern of disease progression, and resemble stages in neurogenesis. *Cancer cell* **9**, 157-173 (2006). https://doi.org:10.1016/j.ccr.2006.02.019
11 Marziali, G. *et al.* Metabolic/Proteomic Signature Defines Two Glioblastoma Subtypes With Different Clinical Outcome. *Scientific reports* **6**, 21557 (2016). https://doi.org:10.1038/srep21557
12 Neftel, C. *et al.* An Integrative Model of Cellular States, Plasticity, and Genetics for Glioblastoma. *Cell* **178**, 835-849 e821 (2019). https://doi.org:10.1016/j.cell.2019.06.024
13 Colman, H. *et al.* A multigene predictor of outcome in glioblastoma. *Neuro-oncology* **12**, 49-57 (2010). https://doi.org:10.1093/neuonc/nop007
14 Segerman, A. *et al.* Clonal Variation in Drug and Radiation Response among Glioma-Initiating Cells Is Linked to Proneural-Mesenchymal Transition. *Cell reports* **17**, 2994-3009 (2016). https://doi.org:10.1016/j.celrep.2016.11.056
15 Lu, F. *et al.* Olig2-Dependent Reciprocal Shift in PDGF and EGF Receptor Signaling Regulates Tumor Phenotype and Mitotic Growth in Malignant Glioma. *Cancer cell* **29**, 669-683 (2016). https://doi.org:10.1016/j.ccell.2016.03.027
16 Ozawa, T. *et al.* Most human non-GCIMP glioblastoma subtypes evolve from a common proneural-like precursor glioma. *Cancer cell* **26**, 288-300 (2014). https://doi.org:10.1016/j.ccr.2014.06.005
17 Fang, X. *et al.* The zinc finger transcription factor ZFX is required for maintaining the tumorigenic potential of glioblastoma stem cells. *Stem cells* **32**, 2033-2047 (2014). https://doi.org:10.1002/stem.1730
18 Fang, X. *et al.* Deubiquitinase USP13 maintains glioblastoma stem cells by antagonizing FBXL14-mediated Myc ubiquitination. *The Journal of experimental medicine* **214**, 245-267 (2017). https://doi.org:10.1084/jem.20151673
19 Li, Z. *et al.* Hypoxia-inducible factors regulate tumorigenic capacity of glioma stem cells. *Cancer cell* **15**, 501-513 (2009). https://doi.org:10.1016/j.ccr.2009.03.018
20 Tao, W. *et al.* Dual Role of WISP1 in maintaining glioma stem cells and tumor-supportive macrophages in glioblastoma. *Nature communications* **11**, 3015 (2020). https://doi.org:10.1038/s41467-020-16827-z
21 Wang, X. *et al.* Purine synthesis promotes maintenance of brain tumor initiating cells in glioma. *Nature neuroscience* **20**, 661-673 (2017). https://doi.org:10.1038/nn.4537
22 Bao, S. *et al.* Targeting cancer stem cells through L1CAM suppresses glioma growth. *Cancer Res* **68**, 6043-6048 (2008). https://doi.org:10.1158/0008-5472.CAN-08-1079
23 Dong, Z. *et al.* Targeting Glioblastoma Stem Cells through Disruption of the Circadian Clock. *Cancer discovery* **9**, 1556-1573 (2019). https://doi.org:10.1158/2159-8290.CD-19-0215

24 Jin, X. *et al.* Targeting glioma stem cells through combined BMI1 and EZH2 inhibition. *Nature medicine* **23**, 1352-1361 (2017). https://doi.org:10.1038/nm.4415

25 Shi, Y. *et al.* Ibrutinib inactivates BMX-STAT3 in glioma stem cells to impair malignant growth and radioresistance. *Science translational medicine* **10** (2018). https://doi.org:10.1126/scitranslmed.aah6816

26 Hjelmeland, A. B. *et al.* Targeting A20 decreases glioma stem cell survival and tumor growth. *PLoS Biol* **8**, e1000319 (2010). https://doi.org:10.1371/journal.pbio.1000319

27 Gimple, R. C., Bhargava, S., Dixit, D. & Rich, J. N. Glioblastoma stem cells: lessons from the tumor hierarchy in a lethal cancer. *Genes & development* **33**, 591-609 (2019). https://doi.org:10.1101/gad.324301.119

28 de The, H. Differentiation therapy revisited. *Nature reviews. Cancer* **18**, 117-127 (2018). https://doi.org:10.1038/nrc.2017.103

29 Storm, E. E. *et al.* Targeting PTPRK-RSPO3 colon tumours promotes differentiation and loss of stem-cell function. *Nature* **529**, 97-100 (2016). https://doi.org:10.1038/nature16466

30 Yan, M. *et al.* IKKalpha restoration via EZH2 suppression induces nasopharyngeal carcinoma differentiation. *Nature communications* **5**, 3661 (2014). https://doi.org:10.1038/ncomms4661

31 Pattabiraman, D. R. W., R. A. . Targeting the epithelial-to-mesenchymal transition: the case for differentiation-based therapy. *Cold Spring Harb. Symp. Quant. Biol.* **81**, 11-19 (2017).

32 Lu, C. *et al.* IDH mutation impairs histone demethylation and results in a block to cell differentiation. *Nature* **483**, 474-478 (2012). https://doi.org:10.1038/nature10860

33 Pusch, S. *et al.* Pan-mutant IDH1 inhibitor BAY 1436032 for effective treatment of IDH1 mutant astrocytoma in vivo. *Acta neuropathologica* **133**, 629-644 (2017). https://doi.org:10.1007/s00401-017-1677-y

34 Li, Y. *et al.* Cholera toxin induces malignant glioma cell differentiation via the PKA/CREB pathway. *Proceedings of the National Academy of Sciences of the United States of America* **104**, 13438-13443 (2007). https://doi.org:10.1073/pnas.0701990104

35 Xing, F. *et al.* The Anti-Warburg Effect Elicited by the cAMP-PGC1alpha Pathway Drives Differentiation of Glioblastoma Cells into Astrocytes. *Cell reports* **18**, 468-481 (2017). https://doi.org:10.1016/j.celrep.2016.12.037

36 Amankulor, N. M. *et al.* Mutant IDH1 regulates the tumor-associated immune system in gliomas. *Genes & development* **31**, 774-786 (2017). https://doi.org:10.1101/gad.294991.116

37 Chen, J. Y. *et al.* The oncometabolite R-2-hydroxyglutarate activates NF-kappaB-dependent tumor-promoting stromal niche for acute myeloid leukemia cells. *Scientific reports* **6**, 32428 (2016). https://doi.org:10.1038/srep32428

38 Lujambio, A. *et al.* Non-cell-autonomous tumor suppression by p53. *Cell* **153**, 449-460 (2013). https://doi.org:10.1016/j.cell.2013.03.020

39 Xue, W. *et al.* Senescence and tumour clearance is triggered by p53 restoration in murine liver carcinomas. *Nature* **445**, 656-660 (2007). https://doi.org:10.1038/nature05529

40 Deshmukh, V. A. *et al.* A regenerative approach to the treatment of multiple sclerosis. *Nature* **502**, 327-332 (2013). https://doi.org:10.1038/nature12647

41 Mei, F. *et al.* Micropillar arrays as a high-throughput screening platform for therapeutics in multiple sclerosis. *Nature medicine* **20**, 954-960 (2014). https://doi.org:10.1038/nm.3618

42 Liu, J. *et al.* Clemastine Enhances Myelination in the Prefrontal Cortex and Rescues Behavioral Changes in Socially Isolated Mice. *The Journal of neuroscience : the official journal of the Society for Neuroscience* **36**, 957-962 (2016). https://doi.org:10.1523/JNEUROSCI.3608-15.2016

43 Hubler, Z. *et al.* Accumulation of 8,9-unsaturated sterols drives oligodendrocyte formation and remyelination. *Nature* **560**, 372-376 (2018). https://doi.org:10.1038/s41586-018-0360-3

44 Green, A. J. *et al.* Clemastine fumarate as a remyelinating therapy for multiple sclerosis (ReBUILD): a randomised, controlled, double-blind, crossover trial. *Lancet* **390**, 2481-2489 (2017). https://doi.org:10.1016/S0140-6736(17)32346-2

45 Moghaddasi, M. *et al.* Randomized control trial of evaluation of Clemastine effects on visual evoked potential, nerve fiber layer and ganglion cell layer complex in patients with optic neuritis. *Clin Neurol Neurosurg* **193**, 105741 (2020). https://doi.org:10.1016/j.clineuro.2020.105741

46 Srikanth, M. *et al.* Nanofiber-mediated inhibition of focal adhesion kinase sensitizes glioma stemlike cells to epidermal growth factor receptor inhibition. *Neuro-oncology* **15**, 319-329 (2013). https://doi.org:10.1093/neuonc/nos316

47 Mao, P. *et al.* Mesenchymal glioma stem cells are maintained by activated glycolytic metabolism involving aldehyde dehydrogenase 1A3. *Proceedings of the National Academy of Sciences of the United States of America* **110**, 8644-8649 (2013). https://doi.org:10.1073/pnas.1221478110

48 Allimuthu, D. *et al.* Diverse Chemical Scaffolds Enhance Oligodendrocyte Formation by Inhibiting CYP51, TM7SF2, or EBP. *Cell Chem Biol* **26**, 593-599 e594 (2019). https://doi.org:10.1016/j.chembiol.2019.01.004

49 Wiese, C. *et al.* Nestin expression--a property of multi-lineage progenitor cells? *Cellular and molecular life sciences : CMLS* **61**, 2510-2522 (2004). https://doi.org:10.1007/s00018-004-4144-6

50 Ellis, P. *et al.* SOX2, a persistent marker for multipotential neural stem cells derived from embryonic stem cells, the embryo or the adult. *Dev Neurosci* **26**, 148-165 (2004). https://doi.org:10.1159/000082134

51 Zhou, Q., Wang, S. & Anderson, D. J. Identification of a novel family of oligodendrocyte lineage-specific basic helix-loop-helix transcription factors. *Neuron* **25**, 331-343 (2000). https://doi.org:10.1016/s0896-6273(00)80898-3

52 Jackson, E. L. *et al.* PDGFR alpha-positive B cells are neural stem cells in the adult SVZ that form glioma-like growths in response to increased PDGF signaling. *Neuron* **51**, 187-199 (2006). https://doi.org:10.1016/j.neuron.2006.06.012

53 Chang, A., Nishiyama, A., Peterson, J., Prineas, J. & Trapp, B. D. NG2-positive oligodendrocyte progenitor cells in adult human brain and multiple sclerosis lesions. *The Journal of neuroscience : the official journal of the Society for Neuroscience* **20**, 6404-6412 (2000).

54 Plemel, J. R., Liu, W.-Q. & Yong, V. W. Remyelination therapies: a new direction and challenge in multiple sclerosis. *Nature Reviews Drug Discovery* **16**, 617-634 (2017). https://doi.org:10.1038/nrd.2017.115

55 Baumann, N. & Pham-Dinh, D. Biology of oligodendrocyte and myelin in the mammalian central nervous system. *Physiol Rev* **81**, 871-927 (2001). https://doi.org:10.1152/physrev.2001.81.2.871

56 Zhang, Y. *et al.* An RNA-sequencing transcriptome and splicing database of glia, neurons, and vascular cells of the cerebral cortex. *The Journal of neuroscience : the official journal of the Society for Neuroscience* **34**, 11929-11947 (2014). https://doi.org:10.1523/JNEUROSCI.1860-14.2014

57 Bhat, M. *et al.* Targeting the translation machinery in cancer. *Nature reviews. Drug discovery* **14**, 261-278 (2015). https://doi.org:10.1038/nrd4505

58 Lee, L. J. *et al.* Cancer Plasticity: The Role of mRNA Translation. *Trends Cancer* **7**, 134-145 (2021). https://doi.org:10.1016/j.trecan.2020.09.005

59 Lathia, J. D., Mack, S. C., Mulkearns-Hubert, E. E., Valentim, C. L. L. & Rich, J. N. Cancer stem cells in glioblastoma. *Genes & development* **29**, 1203-1217 (2015). https://doi.org:10.1101/gad.261982.115

60 Friedmann-Morvinski, D. & Verma, I. M. Dedifferentiation and reprogramming: origins of cancer stem cells. *EMBO reports* **15**, 244-253 (2014). https://doi.org:10.1002/embr.201338254

61 Hu, Y. & Smyth, G. K. ELDA: extreme limiting dilution analysis for comparing depleted and enriched populations in stem cell and other assays. *J Immunol Methods* **347**, 70-78 (2009). https://doi.org:10.1016/j.jim.2009.06.008

62 Kubo, N., Shirakawa, O., Kuno, T. & Tanaka, C. Antimuscarinic effects of antihistamines: quantitative evaluation by receptor-binding assay. *Jpn J Pharmacol* **43**, 277-282 (1987). https://doi.org:10.1254/jjp.43.277

63 Cree, B. A. C. *et al.* Clemastine rescues myelination defects and promotes functional recovery in hypoxic brain injury. *Brain* **141**, 85-98 (2018). https://doi.org:10.1093/brain/awx312

64 Welliver, R. R. *et al.* Muscarinic Receptor M3R Signaling Prevents Efficient Remyelination by Human and Mouse Oligodendrocyte Progenitor Cells. *The Journal of neuroscience : the official journal of the Society for Neuroscience* **38**, 6921-6932 (2018). https://doi.org:10.1523/JNEUROSCI.1862-17.2018

65 Tashiro, M. *et al.* Central effects of fexofenadine and cetirizine: measurement of psychomotor performance, subjective sleepiness, and brain histamine H1-receptor occupancy using 11C-doxepin positron emission tomography. *J Clin Pharmacol* **44**, 890-900 (2004). https://doi.org:10.1177/0091270004267590

66 Brennan, C. W. *et al.* The somatic genomic landscape of glioblastoma. *Cell* **155**, 462-477 (2013). https://doi.org:10.1016/j.cell.2013.09.034

67 Bowman, R. L., Wang, Q., Carro, A., Verhaak, R. G. & Squatrito, M. GlioVis data portal for visualization and analysis of brain tumor expression datasets. *Neuro-oncology* **19**, 139-141 (2017). https://doi.org:10.1093/neuonc/now247

68 Braverman, N. *et al.* Mutations in the gene encoding 3 beta-hydroxysteroid-delta 8, delta 7-isomerase cause X-linked dominant Conradi-Hunermann syndrome. *Nature genetics* **22**, 291-294 (1999). https://doi.org:10.1038/10357

69 Laggner, C. *et al.* Discovery of high-affinity ligands of sigma1 receptor, ERG2, and emopamil binding protein by pharmacophore modeling and virtual screening. *Journal of medicinal chemistry* **48**, 4754-4764 (2005). https://doi.org:10.1021/jm049073+

70 Moebius, F. F. *et al.* Pharmacological analysis of sterol delta8-delta7 isomerase proteins with [3H]ifenprodil. *Mol Pharmacol* **54**, 591-598 (1998). https://doi.org:10.1124/mol.54.3.591

71 Zhang, L. *et al.* Selective targeting of mutant adenomatous polyposis coli (APC) in colorectal cancer. *Science translational medicine* **8**, 361ra140 (2016). https://doi.org:10.1126/scitranslmed.aaf8127

72 Moebius, F. F. *et al.* Histidine77, glutamic acid81, glutamic acid123, threonine126, asparagine194, and tryptophan197 of the human emopamil binding protein are required for in vivo sterol delta 8-delta 7 isomerization. *Biochemistry* **38**, 1119-1127 (1999). https://doi.org:10.1021/bi981804i

73 Herman, G. E. *et al.* Characterization of mutations in 22 females with X-linked dominant chondrodysplasia punctata (Happle syndrome). *Genet Med* **4**, 434-438 (2002). https://doi.org:10.1097/00125817-200211000-00006

74 Long, T. *et al.* Structural basis for human sterol isomerase in cholesterol biosynthesis and multidrug recognition. *Nature communications* **10**, 2452 (2019). https://doi.org:10.1038/s41467-019-10279-w

75 Pirozzi, C. J. *et al.* Mutant IDH1 Disrupts the Mouse Subventricular Zone and Alters Brain Tumor Progression. *Molecular cancer research : MCR* **15**, 507-520 (2017). https://doi.org:10.1158/1541-7786.MCR-16-0485

76 Jonkers, J. *et al.* Synergistic tumor suppressor activity of BRCA2 and p53 in a conditional mouse model for breast cancer. *Nature genetics* **29**, 418-425 (2001). https://doi.org:10.1038/ng747

77 Rahme, G. J., Luikart, B. W., Cheng, C. & Israel, M. A. A recombinant lentiviral PDGF-driven mouse model of proneural glioblastoma. *Neuro-oncology* **20**, 332-342 (2018). https://doi.org:10.1093/neuonc/nox129

78 Tchougounova, E. *et al.* Loss of Arf causes tumor progression of PDGFB-induced oligodendroglioma. *Oncogene* **26**, 6289-6296 (2007). https://doi.org:10.1038/sj.onc.1210455

79 Alessandrini, F. *et al.* Glioblastoma models driven by different mutations converge to the proneural subtype. *Cancer letters* **469**, 447-455 (2020). https://doi.org:10.1016/j.canlet.2019.11.010

80 Becher, O. J. *et al.* Preclinical evaluation of radiation and perifosine in a genetically and histologically accurate model of brainstem glioma. *Cancer Res* **70**, 2548-2557 (2010). https://doi.org:10.1158/0008-5472.CAN-09-2503

81 Lei, L. *et al.* Glioblastoma models reveal the connection between adult glial progenitors and the proneural phenotype. *PloS one* **6**, e20041 (2011). https://doi.org:10.1371/journal.pone.0020041

82 Tarca, A. L. *et al.* A novel signaling pathway impact analysis. *Bioinformatics* **25**, 75-82 (2009). https://doi.org:10.1093/bioinformatics/btn577

83 Le Joncour, V. *et al.* Vulnerability of invasive glioblastoma cells to lysosomal membrane destabilization. *EMBO molecular medicine* **11** (2019). https://doi.org:10.15252/emmm.201809034

84 Guo, D. *et al.* An LXR agonist promotes glioblastoma cell death through inhibition of an EGFR/AKT/SREBP-1/LDLR-dependent pathway. *Cancer discovery* **1**, 442-456 (2011). https://doi.org:10.1158/2159-8290.CD-11-0102

85 Cheng, X. *et al.* Targeting DGAT1 Ameliorates Glioblastoma by Increasing Fat Catabolism and Oxidative Stress. *Cell metabolism* **32**, 229-242 e228 (2020). https://doi.org:10.1016/j.cmet.2020.06.002

86 Geng, F. *et al.* Inhibition of SOAT1 Suppresses Glioblastoma Growth via Blocking SREBP-1-Mediated Lipogenesis. *Clinical cancer research : an official journal of the American Association for Cancer Research* **22**, 5337-5348 (2016). https://doi.org:10.1158/1078-0432.CCR-15-2973

87 Villa, G. R. *et al.* An LXR-Cholesterol Axis Creates a Metabolic Co-Dependency for Brain Cancers. *Cancer cell* **30**, 683-693 (2016). https://doi.org:10.1016/j.ccell.2016.09.008

88 Bi, J. *et al.* Altered cellular metabolism in gliomas - an emerging landscape of actionable co-dependency targets. *Nature reviews. Cancer* **20**, 57-70 (2020). https://doi.org:10.1038/s41568-019-0226-5

89 Phillips, R. E. *et al.* Target identification reveals lanosterol synthase as a vulnerability in glioma. *Proceedings of the National Academy of Sciences of the United States of America* **116**, 7957-7962 (2019). https://doi.org:10.1073/pnas.1820989116

90 Pavlik, E. J. *et al.* Resistance to tamoxifen with persisting sensitivity to estrogen: possible mediation by excessive antiestrogen binding site activity. *Cancer Res* **52**, 4106-4112 (1992).

91 Leignadier, J., Dalenc, F., Poirot, M. & Silvente-Poirot, S. Improving the efficacy of hormone therapy in breast cancer: The role of cholesterol metabolism in SERM-mediated autophagy, cell differentiation and death. *Biochem Pharmacol* **144**, 18-28 (2017). https://doi.org:10.1016/j.bcp.2017.06.120

92 Yang, R. *et al.* Cic loss promotes gliomagenesis via aberrant neural stem cell proliferation and differentiation. *Cancer Res* (2017). https://doi.org:10.1158/0008-5472.CAN-17-1018

93 Nagaraja, S. *et al.* Transcriptional Dependencies in Diffuse Intrinsic Pontine Glioma. *Cancer cell* **31**, 635-652 e636 (2017). https://doi.org:10.1016/j.ccell.2017.03.011

94 Korade, Z. *et al.* The Effect of Small Molecules on Sterol Homeostasis: Measuring 7-Dehydrocholesterol in Dhcr7-Deficient Neuro2a Cells and Human Fibroblasts. *Journal of medicinal chemistry* **59**, 1102-1115 (2016). https://doi.org:10.1021/acs.jmedchem.5b01696

95 David A. Reardon, Y. N., Yoshiki Arakawa, Samuel A. Goldlust, George Ansstas, Jian Mei, Edward Dow, Masataka Seki, Yudai Furuta, Gregory Song, Howard Colman. DSP-0390, an oral emopamil binding protein (EBP) inhibitor, in patients with recurrent high-grade glioma: A first-in-human, phase 1 study. *Meeting Abstract | 2022 ASCO Annual Meeting I* **40** (2022).

96 Hansen, L. J. *et al.* MTAP Loss Promotes Stemness in Glioblastoma and Confers Unique Susceptibility to Purine Starvation. *Cancer Res* **79**, 3383-3394 (2019). https://doi.org:10.1158/0008-5472.CAN-18-1010

97 Singh, S. X. *et al.* Purine Synthesis Inhibitor L-Alanosine Impairs Mitochondrial Function and Stemness of Brain Tumor Initiating Cells. *Biomedicines* **10** (2022). https://doi.org:10.3390/biomedicines10040751

98 Lamprecht, M. R., Sabatini, D. M. & Carpenter, A. E. CellProfiler: free, versatile software for automated biological image analysis. *Biotechniques* **42**, 71-75 (2007). https://doi.org:10.2144/000112257

99 Afgan, E. *et al.* The Galaxy platform for accessible, reproducible and collaborative biomedical analyses: 2018 update. *Nucleic acids research* **46**, W537-W544 (2018). https://doi.org:10.1093/nar/gky379

100 Pertea, M., Kim, D., Pertea, G. M., Leek, J. T. & Salzberg, S. L. Transcript-level expression analysis of RNA-seq experiments with HISAT, StringTie and Ballgown. *Nature protocols* **11**, 1650-1667 (2016). https://doi.org:10.1038/nprot.2016.095

101 Ge, S. X., Jung, D. & Yao, R. ShinyGO: a graphical gene-set enrichment tool for animals and plants. *Bioinformatics* **36**, 2628-2629 (2020). https://doi.org:10.1093/bioinformatics/btz931

102 Subramanian, A. *et al.* Gene set enrichment analysis: a knowledge-based approach for interpreting genome-wide expression profiles. *Proceedings of the National Academy of Sciences of the United States of America* **102**, 15545-15550 (2005). https://doi.org:10.1073/pnas.0506580102

Figure Legends

Fig. 1. Propagation of patient-derived BTIC cultures is suppressed by benztropine and clemastine. (A) Proliferation of BTIC#102 cells treated with clemastine (Clem) at indicated doses. n = 3 per condition except vehicle, n = 9. **(B)** Representative images (4x, scale bar: 400 μm) of BTIC#102 cells treated with vehicle (Veh) or clemastine (Clem; at 4 μM) for 20 days in laminin-coated plates. **(C)** Quantification of cell cycle analysis of BTIC#102 cells treated with clemastine at indicated doses for 12 days. n = 2 per condition. **(D)** Proliferation of BTIC#102 cells with or without 10-day clemastine (4 μM) pre-treatments (pre-Tx) and/or subsequent clemastine (4 μM) treatments (cont. Tx). Cell proliferation was monitored during subsequent clemastine treatments. n = 9 per condition except for the pre-Tx^{+}cont.Tx^{+} group, n = 6. "-": no clemastine in the media; "+": with clemastine in the media. **(E-F)** Quantification of relative cell proliferation of BTICs bearing *EGFR* amplification **(E**, left panel**)**, **or** features of mesenchymal (MES) subtypes (**E**, right panel**)**, or **(F)** normal human astrocytes treated with clemastine (Clem) at indicated doses. The y-axis represents normalized phase area confluence at day 4 (normalized to day 0 and then normalized to respective vehicle controls). n = 12 for all vehicle groups except BTIC#127, n = 6; n = 6 for all drug-treated groups except BTIC#127, n=3. (A, D-F) Data are represented as mean ± S.E.M.. Significance was calculated using two-way repeated measures ANOVA followed by (A) Dunnett's or (D) Tukey's multiple comparisons tests or two-way ANOVA followed by (C) Tukey's or (E-F) Sidak's multiple comparisons tests and represented as *p < 0.05, **p < 0.01, ***p < 0.001, n.s.: not significant.

Fig. 2. Clemastine attenuates the stemness and progenitor cell features of *PDGFRA*$^{+}$ BTICs. (A) mRNA expression levels of genes associated with NSCs, OPCs, oligodendrocytes, and suppressors of OPC differentiation in BTIC#102 cells treated with vehicle or clemastine (4 μM) for 9-15 days as assessed by quantitative RT-PCR. n = 7 per gene except MOG, CSPG5, and NOTCH1, n = 6, NCAN, n = 5, and NES, SOX2, n = 3. **(B-C)** Protein levels of NSC and OPC markers in BTIC#102 cells treated with clemastine at indicated doses for 13-14 days as assessed by **(B)** immunoblot assays (representative results from three independent experiments) or **(C)** immunofluorescence (IF) staining (representative images from two independent experiments; 20x, scale bar: 50 μm). **(D-G)** IF staining of PDGFRA and GALC in BTIC#102 cells treated with vehicle or clemastine (Clem; at 6 μM) for 26 days. **(D)** Representative IF images (20x, scale bar: 50 μm), **(E)** quantification of mean PDGFRA and GALC fluorescence intensities, and **(F)** percentages of $PDGFRA^{+}$ and $GALC^{+}$ cells of the vehicle and clemastine-treated groups. (E-F) Each data point was calculated from a different field of view. n = 22 fields of view for all vehicle groups, and n = 32 for all clemastine-treated groups. **(G)** The contingency

table of PDGFRA$^{-/+}$ and/or GALC$^{-/+}$ cell counts to assess the mutual exclusivity of PDGFRA and GALC positivity. A total of 5804 cells were identified from 54 fields of view. **(H-I)** MA plots summarizing differential mRNA expression of top 40 **(H)** OPC-specific genes or **(I)** oligodendrocytes-specific genes between clemastine versus vehicle-treated (15-day treatment) BTIC#102 cells. Larger symbols indicate genes with adjusted p-values < 0.05. **(J)** Extreme limiting dilution analysis (ELDA) of BTIC#102 cells treated with clemastine (Clem) at indicated doses for 14 days to assess their renewal capacity. P-values indicate significance between vehicle and clemastine-treated groups. **(K)** ELDA of BTIC#102 (left panel) and BTIC#148 (right panel) cells with or without 15-day clemastine (4 μM) pre-treatments (pre-Tx) and/or subsequent two-week clemastine (4 μM) treatments (cont. Tx). P-values indicate significance between the pre-Tx^{-}cont.Tx^{-} group and other groups. n = 4 per condition. "-": no clemastine in the media; "+" with clemastine in the media. Data are represented as (A) geometric mean ± geometric S.D. of fold change relative to vehicle-treated groups or (E-F) mean ± S.E.M.. (E-F) Significance was calculated using unpaired t tests (F left panel with Welch's correction) and represented as *p < 0.05, **p < 0.01, ***p < 0.001, n.s.: not significant.

Fig. 3. EBP is essential for BTIC cell proliferation and its inhibition contributes to clemastine's suppressive effects on BTICs. (A) Proliferation of non-targeting shRNA control (shCtl) and two non-overlapping *EBP* shRNA (sh*EBP*-1 and sh*EBP*-2) BTIC#102 cells 24 hours after lentiviral transduction. n = 6 per condition. **(B)** Representative images (4x, scale bar: 500 μm) of shCtl and sh*EBP*-1 BTIC#102 cells 9 days after lentiviral transduction. **(C)** Proliferation of vector control (pcDNA3.1-Ctl) and *EBP*-overexpressed (pcDNA3.1-*EBP*) BTIC#102 cells. P-values indicate significance between the two groups at indicated timepoints. n = 6 per condition. **(D)** Quantification of relative cell proliferation of BTIC#102 cells with vector control, overexpression of wild-type EBP, or overexpression of each of the three mutant EBPs. The y-axis represents normalized phase area confluence at day 6 (normalized to day 0 and then normalized to respective vehicle controls). n = 12 per condition. **(E)** Proliferation of BTIC#102 cells treated with clemastine (Clem; at 6 μM) with or without water-soluble cholesterol (Chol) at indicated doses. n = 4 per condition. **(F)** Proliferation of BTIC#102 cells treated with clemastine (Clem; at 6 μM) and/or lathosterol (Lath; at 6.25 μM). n = 6 per condition. **(G)** Quantification of relative cell proliferation of vector control and *EBP*-overexpressed BTIC#102 cells treated with clemastine at indicated doses. The y-axis represents normalized phase area confluence at day 4 (normalized to day 0 and then normalized to respective vehicle controls). n = 6 per condition. (A, C-G) Data are represented as mean ± S.E.M.. Significance was calculated using two-way repeated measures ANOVA followed by (A) Dunnett's, (C) Sidak's, or (E-F) Tukey's multiple comparisons tests, (D) ordinary one-way ANOVA

followed by Dunnett's multiple comparisons tests, or (G) two-way ANOVA followed by Sidak's multiple comparisons tests, and represented as *p < 0.05, **p < 0.01, ***p < 0.001, n.s.: not significant.

Fig. 4. A mouse glioma cell line (C266) depends on Ebp for optimal growth and is susceptible to clemastine. (A) Proliferation of non-targeting shRNA control (shCtl) or *Ebp* shRNA (sh*Ebp*) C266 cells 12 days after lentiviral transduction. P-values indicate significance between the two groups at indicated timepoints. n = 18 per condition. **(B)** ELDA of shCtl and sh*Ebp* C266 cells to assess their self-renewal capacity. **(C)** Proliferation of C266 cells treated with CW3388 at indicated doses. n = 6 per condition except vehicle, n = 12. **(D)** Proliferation of C266 cells treated with clemastine (Clem) at indicated doses. n = 6 per condition except vehicle, n = 12. **(E)** Quantification of relative cell proliferation of shCtl and sh*Ebp* C266 cells treated with clemastine (left panel) or CW3388 (right panel) at indicated doses. The y-axis represents normalized phase area confluence at day 4 (normalized to day 0 and then normalized to respective vehicle controls). n = 6 per condition except for all vehicle groups of the clemastine-treated panel, n = 9. **(F-H)** *In vivo* orthotopic xenograft mouse models derived from C266 cells treated with vehicle (30% DMSO in PBS) or clemastine (30 mg/kg) five times per week. **(F)** Quantification of tumor sizes 7 days after the first treatment by *in vivo* bioluminescent imaging, **(G)** Kaplan Meier analyses, and **(H)** average mouse body weight. (G-H) Day 0 on the x-axis indicates the treatment start date. n = 21 mice for the vehicle group and n = 20 mice for the clemastine-treated group. (A, C-F, H) Data are represented as mean ± S.E.M.. Significance was calculated using two-way repeated measures ANOVA followed by (A) Sidak's or (C-D) Dunnett's multiple comparisons tests, (E) two-way ANOVA followed by Sidak's multiple comparisons tests, (F) Mann-Whitney tests, and represented as *p < 0.05, **p < 0.01, ***p < 0.001, n.s.: not significant.

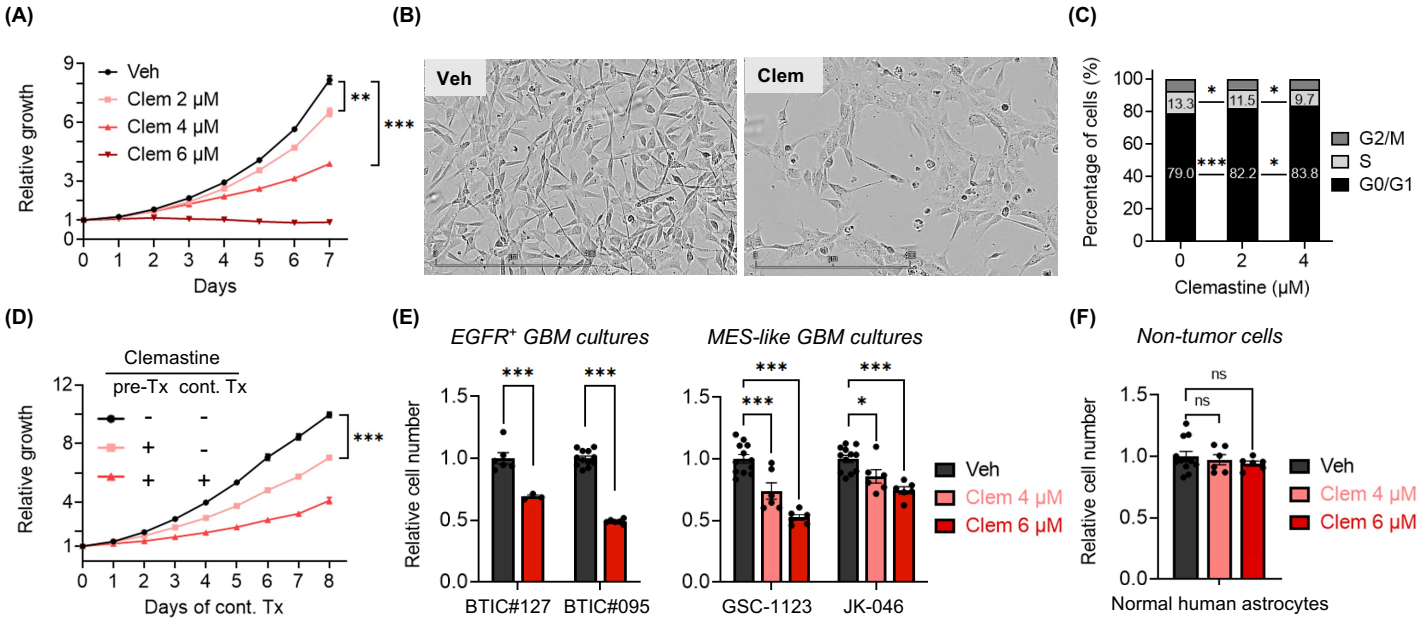

Sun, Yang et al Fig. 1

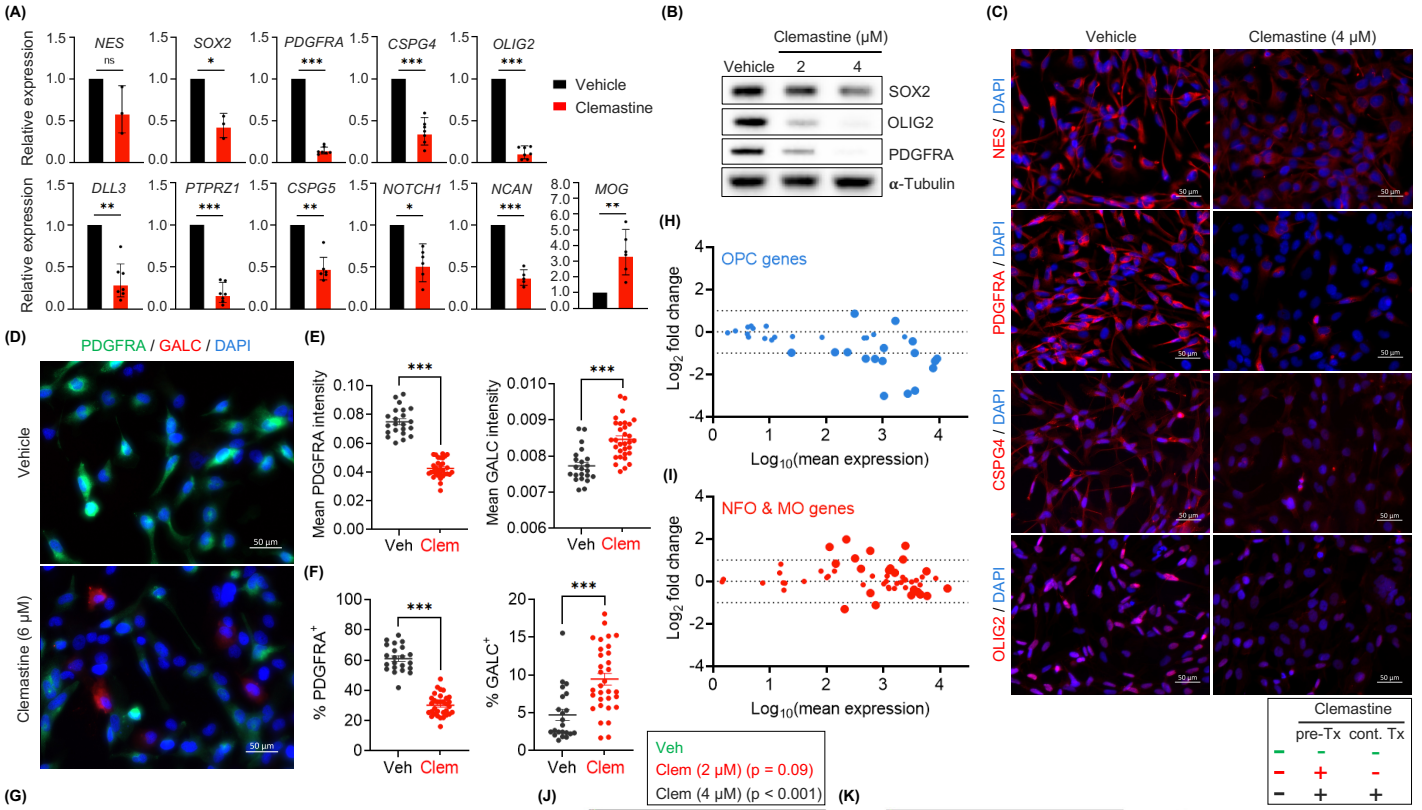

(G)

	GALC-	GALC+	Total	P-value
	number of cells (%)			
PDGFRA-	2969 (51.15)	384 (6.62)	3353 (57.77)	
PDGFRA+	2402 (41.39)	49 (0.84)	2451 (42.23)	< 0.001
Total	5371 (92.54)	433 (7.46)	5804 (100)	

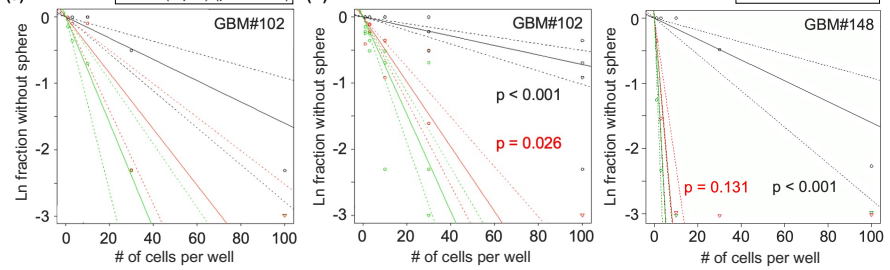

Sun, Yang et al Fig. 2

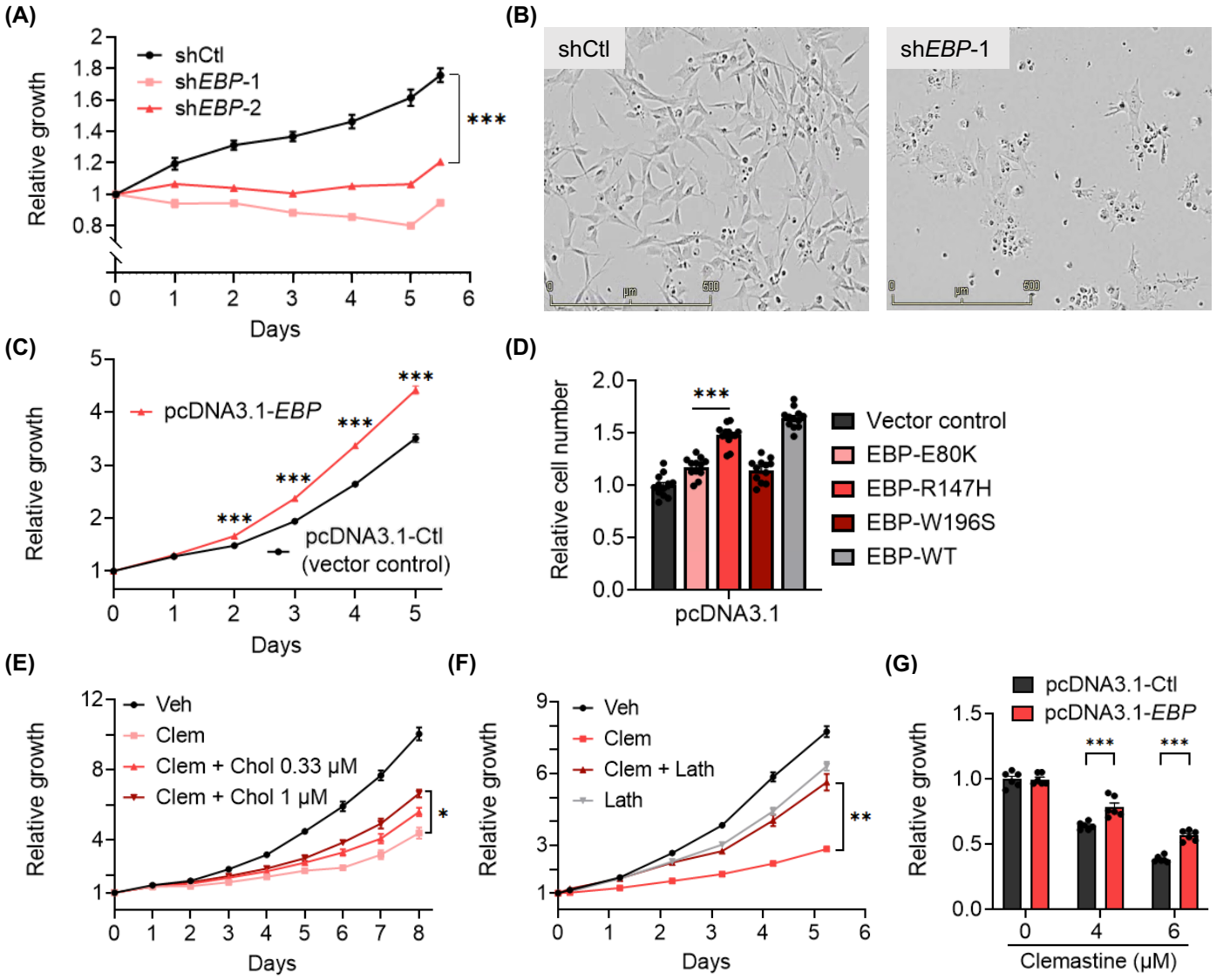

Sun, Yang et al Fig. 3

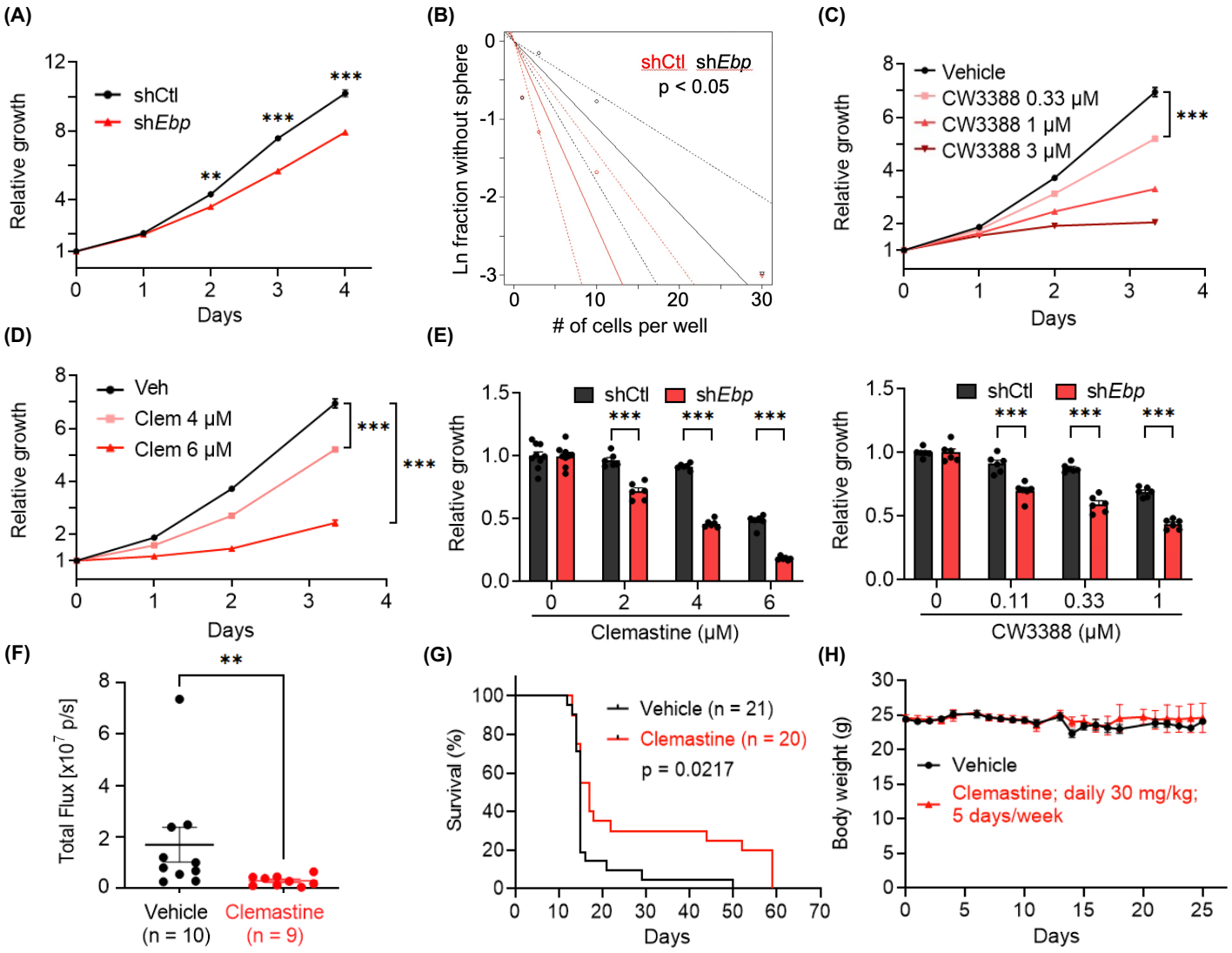

Sun, Yang et al Fig. 4